

---

# Adaptive Nulling in the Hyperthermia Treatment of Cancer

Alan J. Fenn and Gerald A. King

■ We have investigated the use of adaptive array antenna techniques to maximize the applied electric field at a tumor site in a target body while simultaneously minimizing or reducing the field at the locations of undesired high-temperature regions, or hot spots. Computer simulations have shown that adaptive nulling can prevent undesired hot spots from occurring during the heating of a deep-seated tumor. The simulation results have been supported by experimental measurements with a commercial hyperthermia phased-array antenna system that was modified to implement adaptive-nulling and adaptive-focusing algorithms. The experiments were conducted at the State University of New York (SUNY) Health Science Center in Syracuse, N.Y. Two types of phantom targets—a saline-filled polyethylene bottle and a beef sample—were used in the experiments. Results indicate that adaptive nulling can be used to reduce the electric field at one or more target positions while simultaneously maintaining a focus at a deep-seated location within the target.

**T**HE TREATMENT OF deep-seated malignant tumors is often a difficult task, in which the objective is to reduce the size of or completely remove a tumor mass by using one or more modalities. The common modalities are surgery, chemotherapy, and X-ray therapy [1]. A particular modality used alone or in conjunction with another modality is hyperthermia [1–5], in which a tumor is heated to diminish it.

For localized tumor heating, multiple-applicator phased arrays [6, 7] are commonly used to transmit a focused radio frequency (RF) main beam at the tumor site [2, 8]. A commercially available RF hyperthermia system is shown in Figure 1. Manufactured by BSD Medical Corp. of Salt Lake City, Utah, the BSD-2000 Sigma-60 is an annular phased-array antenna system that uses eight uniformly spaced dipole elements [9, 10]. The eight transmit elements are fed as four pairs and each of the four active channels has an electronically controlled variable-phase shifter that

can be used to focus the array antenna. Note that the annular phased-array antenna fully surrounds the patient, enabling constructive interference (or signal enhancement) deep within the patient's body. Temperature and electric-field probe sensors (both invasive and noninvasive) are used to monitor the treatment.

For hyperthermia to have therapeutic value, a controlled thermal dose distribution is required. Typical localized temperatures necessary for therapeutic hyperthermia treatment of cancer range from 42.5° to 45°C. (The normal temperature of human tissue is 37°C.) The most difficult aspect of implementing hyperthermia with either RF or acoustic (ultrasound) waves is producing sufficient heating at the site of a deep-seated tumor. Ideally, a focal region is concentrated at the tumor with minimal energy delivered to the surrounding healthy tissue, which should be kept at temperatures below 42.5°C. But a major problem in heating a deep-seated tumor with a hyperthermia antenna is the formation of undesired hot spots in the



**FIGURE 1.** BSD-2000 hyperthermia system. The 59-cm-diameter annular antenna consists of eight dipoles that are fed as four active pairs of elements. The system operates over the frequency band from 60 to 120 MHz with up to 500 W average power per channel. A cool water ( $5^{\circ}$  to  $40^{\circ}\text{C}$ ) bolus between the patient and the annular array prevents excess heating of the skin surface.

surrounding tissue. The hot spots can result in pain, burns, and blistering, requiring the termination of treatment. Thus techniques for reducing hot spots are necessary for effective hyperthermia treatment. This article investigates the use of adaptive nulling to reduce such undesired hyperthermia-induced hot spots.

Adaptive nulling is a feedback process that can be used by an antenna system to control its receive (or transmit) pattern for optimum reception (or transmission). In the communications and radar fields, adaptive nulling has been successfully used by array antennas to place nulls in the direction of interference sources, thereby minimizing the degradation caused by the interference [11, 12]. There are two major similarities between the radar application and RF hyperthermia: (1) phased-array near-field focusing is used to form the main beam and (2) uncontrolled electric fields or high sidelobes are potentially deleterious to system performance. In radar systems, interference signals entering through uncontrolled sidelobes can reduce the signal-to-noise ratio (SNR); adaptive nulling is commonly used to counteract this possible degradation. In hyperthermia systems, high-transmit antenna electric fields can result in un-

desired hot spots in the target tissue; adaptive nulling of the electric field near the locations of the hot spots could be used to alleviate such high-temperature regions.

Many studies have been conducted to obtain improved therapeutic field distributions with hyperthermia phased arrays [13–30]. Amplitude and phase control can be used to synthesize improved RF radiation patterns without adaptive control of the transmit-array weights [13–20]. Array transmit weights can be adaptively controlled to maximize the tumor temperature (or RF power delivered to the tumor) while minimizing the surrounding tissue temperature (or RF power delivered to the surrounding tissue) [21–30]. All the above studies require invasive techniques to optimize the radiation pattern.

The work described in this article emphasizes two features that the research cited in the previous paragraph does not consider. First, the electric field is minimized or maximized at specified locations with electric-field sensors at those locations. The signals received by the sensors are used as feedback to an adaptive algorithm. Second, the work described in this article emphasizes noninvasive adaptive nulling for eliminating hot spots within the target body near

its surface. Recently, the application of near-field adaptive-array techniques [31–34] to RF hyperthermia for deep-seated tumor therapy has been investigated at Lincoln Laboratory. With computer simulations, it has been shown that adaptive nulling with noninvasive auxiliary dipole sensors can theoretically be used to reduce the field intensity at selected positions in the target body while maintaining a desired focus at a tumor site [35–39]. In the simulations, the electric field radiated by an RF hyperthermia phased array was minimized (nulled) at multiple hot-spot locations and maximized (focused) at desired target positions by adaptively adjusting the transmit amplifiers and phase shifters of the hyperthermia apparatus. The simulations were for a homogeneous elliptical phantom target surrounded by a water bolus and hyperthermia ring array.

We have supported the simulation results with experimental measurements. Currently, clinical operation of the BSD-2000 system of Figure 1 allows only limited manual control of the array transmit-element amplitude and phase. Some improvement in the electric-field distribution can be achieved by this manual trial-and-error method [13, 14], but automatic adjustment techniques that are offered by adaptive arrays are desirable; such techniques have the potential for therapeutically better electric-field distributions. Using a modified version of the BSD-2000 in which adaptive techniques were implemented with a gradient-search algorithm, we have demonstrated adaptive focusing and adaptive nulling at multiple target locations [40, 41]. In the experiments, which were conducted at the State University of New York (SUNY) Health Science Center in Syracuse, N.Y., we used two types of phantom targets—a saline-filled polyethylene bottle and a beef sample.

The remainder of this article is organized as follows. The section “Theory” discusses the concept for a noninvasive adaptive hyperthermia system and describes algorithms used in implementing the adaptive array. In the section “Simulation Results,” a brief summary of the results obtained with the computer modeling of a hyperthermia system is given. The section “Experimental Results” first describes the materials and methods used in the experiments con-

ducted at SUNY, and then gives results for the modified BSD-2000, an adaptive four-channel hyperthermia ring array, operating at continuous wave (CW) frequencies of 100 and 120 MHz. The received RF-power distributions measured by short-dipole field probes both before and after adaptive nulling are presented for the saline-filled polyethylene bottle and the beef sample used.

## Theory

### *Noninvasive Adaptive Hyperthermia System Concept*

The concept of a noninvasive adaptive-nulling hyperthermia system for a simplified target body is shown in Figure 2. For generating the desired electric-field distribution in a clinical adaptive hyperthermia system, receiving sensors are positioned as closely as possible to the focus (i.e., tumor site) and where high temperatures are to be avoided, such as near the spinal cord and scar tissue. In a noninvasive adaptive-nulling system, the auxiliary sensors 1, 2, . . . ,  $N_{\text{aux}}$  are placed on the target skin as shown. The finite-width null zones centered at each auxiliary probe extend naturally into the elliptical target region to eliminate undesired hot spots. The width (or extent) of each null zone is directly related to the strength of each null, and the strength of each null (sometimes referred to as the amount of cancellation) is directly related to the SNR at the sensor position. A low SNR results in a small amount of nulling while a high SNR results in a large amount of nulling. The resolution, or minimum spacing, between the focus and null positions is normally equal to the half-power beamwidth of the antenna [42]. The resolution can be enhanced somewhat by using weak nulls whenever the separation between the null and focus is closer than the half-power beamwidth. The focal-spot size, or resolution, of a ring array is approximately one-half the wavelength in the target body [41].

Initially, the hyperthermia array is adaptively focused to produce the required field intensity at the tumor site. An invasive probe is used to obtain the optimum focus at the desired depth. To avoid hot spots, it is necessary to minimize the power received at the selected null positions while constraining the array weights so that the required amount of power is delivered to the tumor site. The adaptive array weights

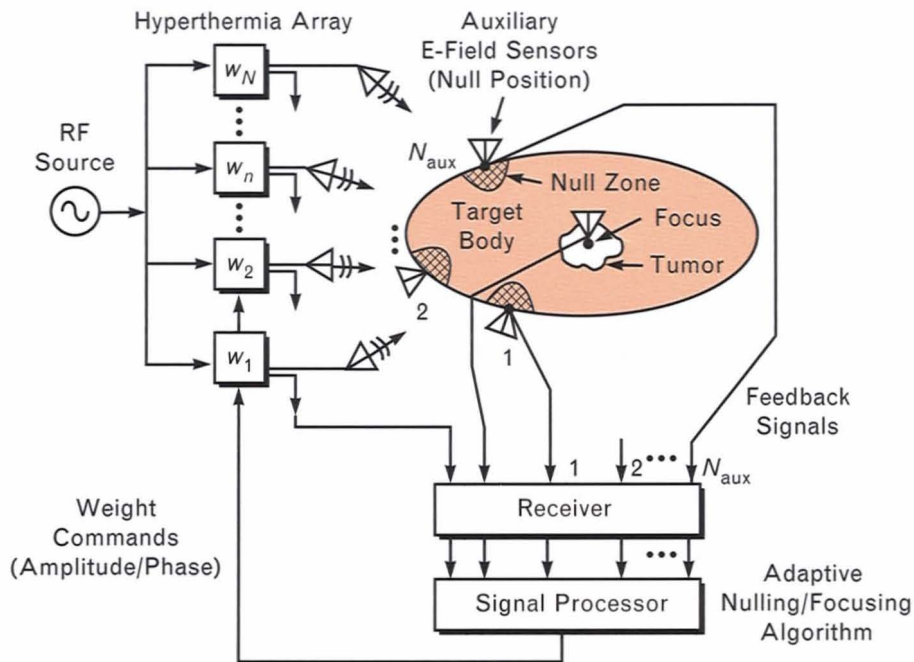


**FIGURE 2.** Concept for noninvasive adaptive hyperthermia system.

(with amplitude  $A$  and phase  $\phi$ ) are controlled by either the sample matrix inversion (SMI) algorithm or a gradient-search algorithm to form the nulls quickly before a significant amount of heating occurs. With this adaptive technique, it should be possible to avoid hot spots while maintaining a therapeutic thermal dose distribution at the tumor site.

*Adaptive Transmit-Array Formulation*

Consider a hyperthermia array with  $N$  identical antenna elements. (Note: For the BSD-2000 system,  $N$  will represent  $N$  pairs of identical antenna elements.) The input signal to each of the  $N$  array elements is obtained from the amplitude- and phase-weighted CW signal distributed by a power divider network. The variable  $N$  also denotes the number of adaptive channels; thus the adaptive-channel weight vector shown in Figure 2 can be given by  $\mathbf{w} = (w_1, w_2, \dots, w_N)^T$ . (The superscript T indicates transpose.)

For an adaptive annular array focused at the origin in homogeneous tissue, the normalized quiescent weight vector is simply  $\mathbf{w}_{\text{quiescent}} = (1, 1, 1, \dots, 1)^T$ ; i.e., the amplitude and phase illumination are uniform. Commonly, the weight vector is constrained to

deliver a required amount of power to the hyperthermia array or to the tumor. For simplicity in the experimental adaptive-hyperthermia-array control software, we constrained the weights such that

$$\sum_{n=1}^N |w_n| = K,$$

where  $|w_n|$  is the transmit-weight amplitude for the  $n$ th adaptive channel and  $K$  is a constant.

The transmit weights (amplitude and phase) can be controlled by either the SMI algorithm or a gradient-search algorithm to generate adaptive nulls. The SMI algorithm has the flexibility to operate in either open- or closed-loop feedback modes [43]; the gradient-search algorithm operates only in a closed-loop feedback mode. The SMI algorithm is also potentially faster. The speed of convergence of the SMI algorithm depends on the number of data samples of the interference. For an  $N$ -channel adaptive array,  $5N$  samples of each channel are typically required to estimate the sample cross-correlation matrix and cancel the interference to within 1 dB of the optimum value obtained with the exact channel-cross-correlation ma-

trix. The speed of convergence of gradient-search algorithms, on the other hand, is highly dependent on the number of interference signals and the difference between their SNRs.

### *Sample Matrix Inversion (SMI) Algorithm*

The SMI algorithm is used to determine the array antenna's transmit-weight settings that will adaptively null interference signals. With the SMI algorithm, a cross-correlation matrix  $\mathbf{R}$  is determined from sampled data and, after matrix inversion, the adaptive-array transmit-weight vector  $\mathbf{w}_{\text{adapted}}$  is calculated as

$$\mathbf{w}_{\text{adapted}} = \mathbf{R}^{-1} \mathbf{w}_{\text{quiescent}}, \quad (1)$$

where  $\mathbf{w}_{\text{quiescent}}$  is the quiescent weight vector and  $^{-1}$  denotes inverse. Calculation of the cross-correlation matrix  $\mathbf{R}$  requires knowledge of the complex received voltages at the auxiliary-probe locations. References 12 and 39 describe further details of the SMI algorithm.

### *Gradient-Search Algorithm*

Gradient-search algorithms are commonly used in adaptive-array applications in which the adaptive-channel cross correlation cannot be calculated or measured. With a gradient search, only the output power of the receiver channels needs to be measured and is used as a feedback signal to the algorithm. A wide variety of gradient searches are possible [44–50].

Under conditions in which only the probe received power is measured (as in the BSD-2000 system), a gradient-search algorithm can be used to minimize the received power at selected positions. A gradient search can help control the transmit weights iteratively to minimize the RF signal received by the probe array. The transmit-array weights (amplitude and phase) are adaptively changed in small increments and the probe-array received power is monitored to determine those weight settings which reduce the received power most rapidly to a null. The mathematical formulation for the gradient search can be developed in a straightforward manner and is described in detail elsewhere [41, 44]; only a brief description will be given in this article. (Note: Although the mathematical formulation is given as a minimization problem, the equations are readily

converted to the maximization case.)

The summation of the power received at the electric-field probes is denoted by  $p$ . The adaptive-array cancellation ratio, denoted by  $C$ , is defined here as the ratio of the summation of probe-received power after adaption to the summation of probe-received power before adaption; i.e.,

$$C = \frac{p_{\text{after}}}{p_{\text{before}}}.$$

Consider now  $J$  sets (or iterations) of  $N$  transmit weights that are applied to an adaptive hyperthermia phased-array antenna. In terms of adaptive nulling, the optimum transmit-weight settings (from the collection of  $J$  sets of  $N$  transmit weights) occur when the total power received by the auxiliary probe array, denoted by  $p$ , is minimized. We employ a method of steepest-descent gradient search to find the optimum transmit weights to minimize  $p$ ; i.e.,

$$p_{\text{optimum}} = \min(p_j) \quad j = 1, 2, \dots, J.$$

Assume that there are  $N$  complex transmit weights in the hyperthermia phased array. The  $m$ th transmit weight in the  $j$ th configuration (or iteration) of transmit weights is denoted by

$$w_{nj} = A_{nj} e^{j\phi_{nj}},$$

where  $A_{nj}$  is the transmit-weight amplitude distributed over the range  $A_{\text{min}}$  to  $A_{\text{max}}$  and  $\phi_{nj}$  is the transmit-weight phase distributed over the range  $\phi_{\text{min}}$  to  $\phi_{\text{max}}$ . The goal is to find the values of amplitude and phase for each of the  $N$  transmit weights such that  $p$  is minimized. When the auxiliary receive array power is minimized, adaptive radiation-pattern nulls will be formed at the auxiliary sensor positions.

Assuming an initial setting of the  $N$  transmit weights, we adjust the weights by dithering them in small increments  $\pm\Delta A_n$  and  $\pm\Delta\phi_n$  until the optimum power is achieved. The goal is to find the collective amplitude and phase search directions for the  $N$  transmit weights such that  $p$  decreases most rapidly. Further details of the gradient search are given in Reference 41.

For adaptive focusing at a tumor site, we employ a

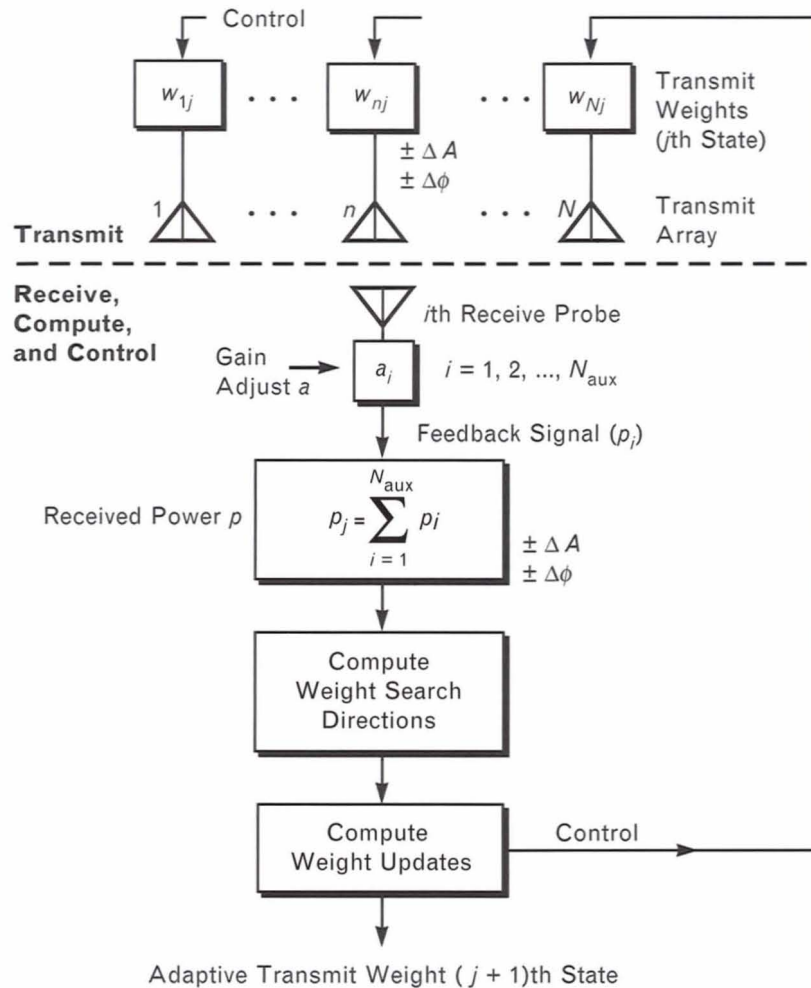


**FIGURE 3.** Block diagram of gradient-search algorithm for adaptive-nulling hyperthermia system.

method of steepest-ascent gradient search to find the optimum transmit weights to maximize  $p$ ; i.e.,

$$p_{\text{optimum}} = \max(p_j) \quad j = 1, 2, \dots, J.$$

For the current software implementation of the gradient search in these experiments, assume (for convenience) that the step sizes are independent of both the iteration number and the adaptive-channel number; i.e.,

$$\Delta A_{nj} = \Delta A, \text{ and}$$

$$\Delta \phi_{nj} = \Delta \phi.$$

In some situations it may be desirable to change the

step size at each iteration [45, 48], but that possibility has not been explored in these measurements.

Figure 3 shows a block diagram for an adaptive hyperthermia system controlled by the gradient-search algorithm. The transmit weights  $w_{1j}, \dots, w_{nj}, \dots, w_{Nj}$  at the  $j$ th iteration are shown at the top of the figure. The transmit phased-array antenna induces a voltage across the terminals of the  $i$ th receive probe antenna. For any given configuration of the transmit weights, each weight is dithered by a small negative and positive amount in amplitude and phase and the received powers at the electric-field probes are stored in the computer for calculation of the total received probe array power, amplitude and phase search direc-

tions, and updated  $(j + 1)$ th transmit-weight configuration. The weight dithering of one transmit weight must be done with the remaining transmit weights in their  $j$ th state. The adaptive weight vector  $\mathbf{w}_{\text{adapted}}$  is achieved when the  $(j + 1)$ th weight configuration has converged. The rate of convergence depends on the number of independently generated adaptive nulls, the SNR at each null position, and the gradient step sizes.

### Simulation Results

Computer simulations at Lincoln Laboratory have shown that the electric field radiated by an RF hyperthermia phased array can be minimized (nulled) at multiple hot-spot locations and maximized (focused) at desired target positions by adaptively adjusting the transmit amplifiers and phase shifters of the hyperthermia apparatus. The simulation results are based on the computation of the electric field with a homogeneous moment-method model

[51–53], and on a transient thermal-analysis computer program [54].

The computer simulation analyzes adaptive nulling with a hyperthermia phased array in an infinite homogeneous conducting medium. The method of moments helps compute the electric field received at a short-dipole sensor due to a radiating thin-wire dipole ring array. The SMI algorithm is used for the adaptive control of the transmit array weights to form the radiation-pattern nulls. The transient thermal behavior of the RF-illuminated target is analyzed with an equivalent electric circuit network similar to the approach used in Reference 55. For a detailed discussion of the computer simulation, see Reference 39.

Figure 4 summarizes the thermal simulation for a 120-MHz RF hyperthermia ring array with eight adaptively controlled dipole elements transmitting uniformly, in amplitude and phase, through a constant-temperature water bolus into a homogeneous elliptical target region. The tumor site is assumed to

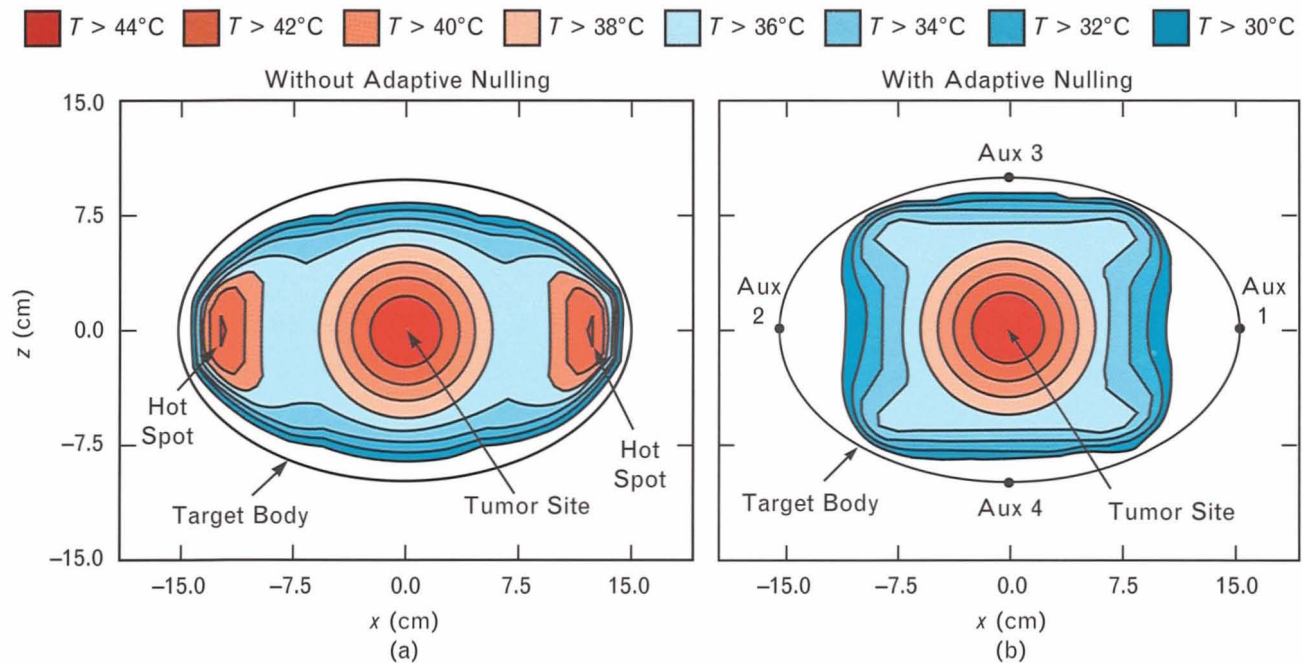


**FIGURE 4.** Simulated two-dimensional thermal pattern: (a) without adaptive nulling and (b) with adaptive nulling at four auxiliary sites. The data are for an eight-element dipole ring array (60-cm diameter) and an elliptical phantom muscle-tissue target surrounded with a water bolus. The incident radio frequency (RF) power distribution is at 120 MHz, the initial temperature of the phantom is 25°C, the relative dielectric constant and electrical conductivity of the phantom muscle tissue are 73.5 and 0.5 Siemens/m, respectively, and the array has been focused at the center of the elliptical target for 20 min. During the simulation, the temperature of the water bolus was held constant at 10°C, and the maximum temperature of the phantom was 46°C. Note that adaptive nulling has eliminated the undesired hot spots on the left and right sides of the target.

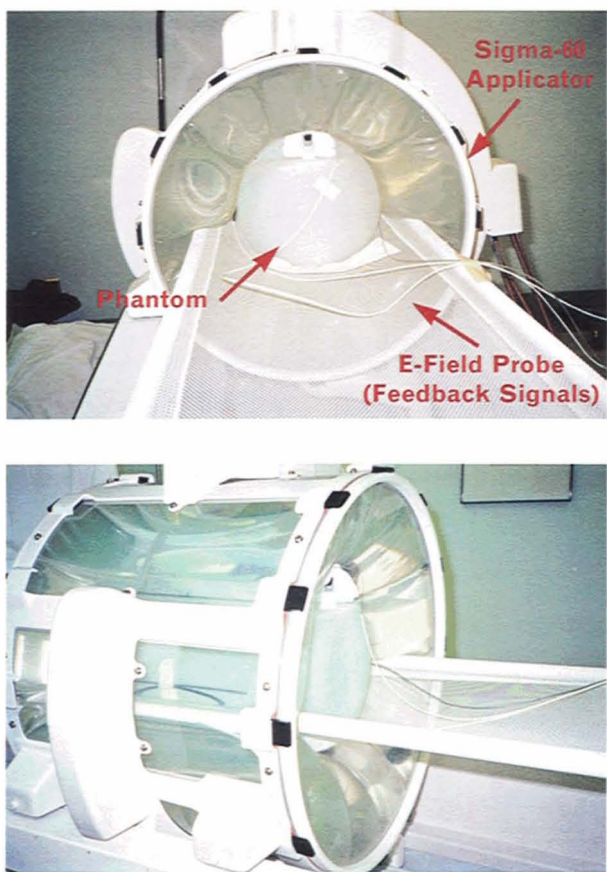


**FIGURE 5.** Experimental setup for the saline-filled cylindrical phantom. Three probes are used to monitor the electric field during the adaptive-nulling measurements.

be at the center of the ellipse. The thermal distribution in Figure 4(a) contains two undesired hot spots, one on either side of the focus. (Note: A similar thermal distribution has been reported in the literature, for example, by S.B. Field and J.W. Hand [2]). The adaptive array weights have been computed from Equation 1. In Figure 4(b), adaptive nulling at four independent positions on the surface of the target body has been applied and, due to the finite widths of the nulls, the undesired hot spots near the surface of the target body have been eliminated. For a detailed discussion of the simulation results, see References 36 through 39.

## Experimental Results

### *Materials and Methods*

The hyperthermia phased-array system used in our experiments at the State University of New York

(SUNY) Health Science Center in Syracuse, N.Y., was the BSD-2000 with Sigma-60 applicator, manufactured by BSD Medical Corp. The system's annular array applicator has a diameter of 59 cm with eight uniformly spaced dipole elements (dipole length of 44 cm) operating over the frequency band from 60 to 120 MHz [10]. The eight dipoles are fed as four active pairs of elements with an average power per channel of up to 500 W. To phase-focus the array, each of the four active channels has an electronically controlled variable-phase shifter. The variable transmit amplitude and phase modules are controlled by digital to analog (D/A) converters. A bolus filled with circulating deionized water, which has a very low RF propagation loss, prevents excess heating of the surface of the patient's skin.

For the electric-field probes, short dipoles with semiconductor diode detectors [56–58] were used. We selected three models of BSD probes: for invasive electric-field measurements, the EP-500 probe; and, for noninvasive electric-field measurements, the EP-100 and EP-400. The lengths of the probe dipole antennas are 1 cm and 3 cm for the EP-500 and the EP-100, respectively, and the EP-400 is a three-element array of dipoles with a total length of 23 cm. (Note: The design of the EP-500 probe is given in Reference 58. For the EP-500 design, the short metallic leads of a Schottky diode are connected between two highly resistive conductive leads. A 1-cm-long conducting wire is added to one of the resistive leads and responds to linear polarization. The leads of the diode and the additional conducting wire act as an offset-feed dipole antenna.) In addition to the electric-field probes, two temperature probes (provided with the BSD-2000 system) were used to monitor the temperature of the beef phantom.

The BSD-2000 comes equipped with eight EP-400 noninvasive electric-field probes for monitoring clinical hyperthermia treatments. The eight EP-400 probes (or, alternatively, eight EP-100 probes) could provide feedback signals to the adaptive algorithm. In theory, with four transmit channels three independent adaptive nulls can be formed with any three of the eight feedback signals.

There are various methods to select the desired null sites. The adaptive algorithm could minimize the

three largest measured electric-field signals on the surface of the patient's skin. If two or three positions are identified as potential hot spots, adaptive nulls could be automatically formed at those positions. Alternatively, if during the heating therapy the patient can localize a painful tissue area, the nearest electric-field probe can be used as the feedback signal to the adaptive-nulling algorithm. In some situations, more than three independent adaptive nulls may be needed to produce a therapeutic thermal distribution. An extension of the present four-channel BSD-2000 Sigma-60 system to eight channels would provide up to seven independent adaptive nulls in addition to a desired focus.

A computer program that implements the gradient-search algorithm was developed at Lincoln Laboratory and integrated at SUNY with the BSD Medical Corp. software for transmit amplitude/phase control and temperature/electric-field monitoring. The integrated MIT/SUNY software allows a user to run either adaptive-nulling or adaptive-focusing algorithms and to monitor the output power of the electric-field probes during the gradient search. The adaptive-nulling algorithm uses phase and amplitude control to form nulls; the adaptive-focusing algorithm uses only phase control to maximize the focal-point electric field. Because the adaptive-array transmit amplifiers and phase shifters are updated continuously, patient breathing and motion should not affect the performance of the feedback algorithms.

The gradient-search algorithm was chosen because the BSD-2000 system measures the applied electric-

field amplitude but not the phase. A potentially better approach to performing adaptive hyperthermia is to use a channel-cross-correlation-matrix-based algorithm (such as the SMI algorithm) and suitable transmit calibration to control the transmitter channels. If both the electric-field phase and amplitude could be measured (e.g., by modification of the electric-field probe hardware to form inphase and quadrature signals), the SMI algorithm could be used to form the nulls.

Phantom, or simulated, human tissue models are commonly used to evaluate hyperthermia techniques [59]. Photographs of the saline-filled phantom that was used in the experiments are shown in Figure 5. The phantom was a 6-gallon cylindrical polyethylene bottle (28-cm diameter and 40-cm length) filled with 0.9% NaCl in deionized water. (Note: The estimated dielectric properties of the various materials used in these experiments are given in Table 1.) Three electric-field probes monitored the electric-field distribution: one probe was mounted invasively at the center of the cylindrical phantom and the other two were mounted separately on the left and right sides of the phantom. The power measured at the invasive probe site was assumed to be the power that would have been delivered to a tumor site.

The beef phantom was a tapered cut of meat obtained from the hind leg just below the knee (Figures 6 and 7). The front face of the beef cut had a horizontal width of 38 cm and a vertical height of 23 cm. Altogether, the beef cut weighed 10.9 kg and had a thickness of 15 cm. The probe positions used in the

**Table 1. Dielectric Properties of Materials Used in the Experiments**

<i>Material</i>	<i>Relative Dielectric Constant</i>	<i>Electrical Conductivity (Siemens/m)</i>
Deionized water	78.0	0.0001
0.9%-NaCl solution	75.0	1.5
Polyethylene	2.25	0.0002
Beef tissue	50.0	1.0
Fat	7.5	0.067
Bone	7.5	0.067

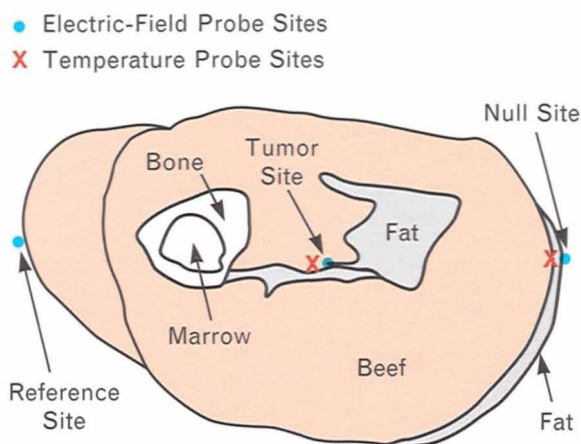


**FIGURE 6.** Front view of the beef phantom used in the experiments. The locations of the electric-field and temperature probes are shown.

experiments are indicated in the figures. As with the saline-filled phantom, three electric-field probes monitored the electric-field distribution: one probe was mounted invasively at the center of the beef phantom and the other two probes were mounted separately on the left and right sides. The power measured at the invasive probe site was assumed to be the power that would have been delivered to a tumor site.

### Results

This subsection presents measured data for the saline-filled cylindrical phantom and the beef phantom. The transmit frequencies used were 100 MHz for the cylindrical phantom and 120 MHz for the beef phantom. The frequencies were selected by monitoring the reflected-power level of the transmitter channels as a function of frequency. Trial and error determined frequencies at which the reflected power was low.

In the first experiment, two adaptive nulls were formed independently on the left and right sides of the cylindrical phantom while the power received at the tumor site was monitored. The longitudinal characteristics of one of the adaptive nulls were quantified by measurement. In the second experiment, an adaptive-focusing gradient search was run for the cylindrical phantom. The focus was positioned on the surface of the phantom. In the third experiment, one adaptive null was formed on the side of the beef sample.

Thermocouple data were measured for this case.

In the following results, the measured electric-field probe A/D-converter data have been converted to power in dB by computing  $10 \log(p)$ , where  $p$  is the value (measured power) of the A/D converter.

*Two adaptive nulls for cylindrical phantom.* In the first experiment, two adaptive nulls were formed simultaneously at two independent electric-field-probe feedback positions. The invasive EP-500 probe was mounted in the center of the cylindrical phantom (the probe was inserted in a catheter through the rubber plug on top of the phantom) to measure the electric-field power at the simulated tumor site. One EP-100 probe was taped to the left side of the phantom and another EP-100 was taped to the right side; the two probes measured the adaptive-nulling feedback signals.

A 50-iteration adaptive-nulling gradient search was executed for this experiment. The commanded initial transmit forward powers on channels 1 through 4 were all 215 W. (The numbering of transmit-array elements 1, 2, 3, and 4 correspond to the anterior, posterior, left, and right quadrants, respectively, as depicted in Figure 8. Note that the *right* side refers to the side of the Sigma-60 that contains the coaxial feed cables.) The commanded initial phase shifts for the four quadrants were all  $89^\circ$ . After 50 iterations of the adaptive-nulling algorithm, the transmit forward powers were 510 W, 55 W, 190 W, and 76 W in quadrants 1 through 4, respectively, and the corresponding phase shifts were  $0^\circ$ ,  $99^\circ$ ,  $58^\circ$ , and  $101^\circ$ , respectively. The measured electric field as a function of iteration number is displayed in Figure 8. Three curves have been plotted; each curve has been normalized to 0 dB at the initial iteration. The two null-site probe powers decrease nearly monotonically over the 50 iterations. At iteration 50, the powers for null-site probes 2 and 3 are  $-18.0$  dB and  $-11.5$  dB, respectively. The tumor-site probe power stays relatively constant during the 50 iterations. With the two symmetric nulls, the main beam tends to stay centered at the desired focus.

Using the adaptive weights from iteration 50, we measured the electric field in the vicinity of one of the nulls. Probe 3 was moved longitudinally and uniformly to nine positions on the surface of the cylindrical phantom; the nine positions scanned 20 cm.

The electric field before and after nulling is presented in Figure 9. Before nulling, the radiation pattern had broad coverage and the half-power beamwidth was at least 20 cm. After nulling, the electric field was reduced at each measurement position over the 20-cm distance. The electric field tended to increase as the probe moved away from the null position at  $y = 0$ . This measured result is consistent with computer simulations in which a longitudinally finite-width null was observed [39].

*Adaptive focus for cylindrical phantom.* In the second experiment, an adaptive focus was formed on the surface of the cylindrical phantom (Figure 10). One EP-100 probe was taped to the right side of the phantom to measure the adaptive-focusing feedback signal at that location. A 30-iteration adaptive-phase-focusing gradient search was executed for this experiment. The initial transmit forward powers on channels 1 through 4 were all 215 W, and the corresponding phase shifts were all  $100^\circ$ . After 30 iterations of the focusing algorithm, the transmit forward powers were held constant and the phase shifts for channels 1

through 4 were  $13^\circ$ ,  $98^\circ$ ,  $78^\circ$ , and  $30^\circ$ , respectively. The measured electric field as a function of iteration number is displayed in Figure 10. Note that the focal-probe power increases by 0.8 dB over the 30 iterations and that the data indicate convergence in about 15 iterations.

*One adaptive null for beef phantom.* The third experiment demonstrated the formation of one adaptive null for the beef phantom. The invasive EP-500 probe was mounted in the center of the phantom, and an EP-400 probe and EP-100 probe were taped to the left and right sides of the phantom, respectively, as shown in Figure 11. The EP-500 measured the electric-field power at the simulated tumor site, the EP-400 measured a reference electric field, and the EP-100 measured the adaptive-nulling feedback signal. A 50-iteration adaptive-nulling gradient search was executed for this experiment, which used a transmit frequency of 120 MHz. The initial transmit forward powers on channels 1 through 4 were all 215 W, and the corresponding phase shifts were all  $103^\circ$ . After 50 iterations of the nulling algorithm, the trans-

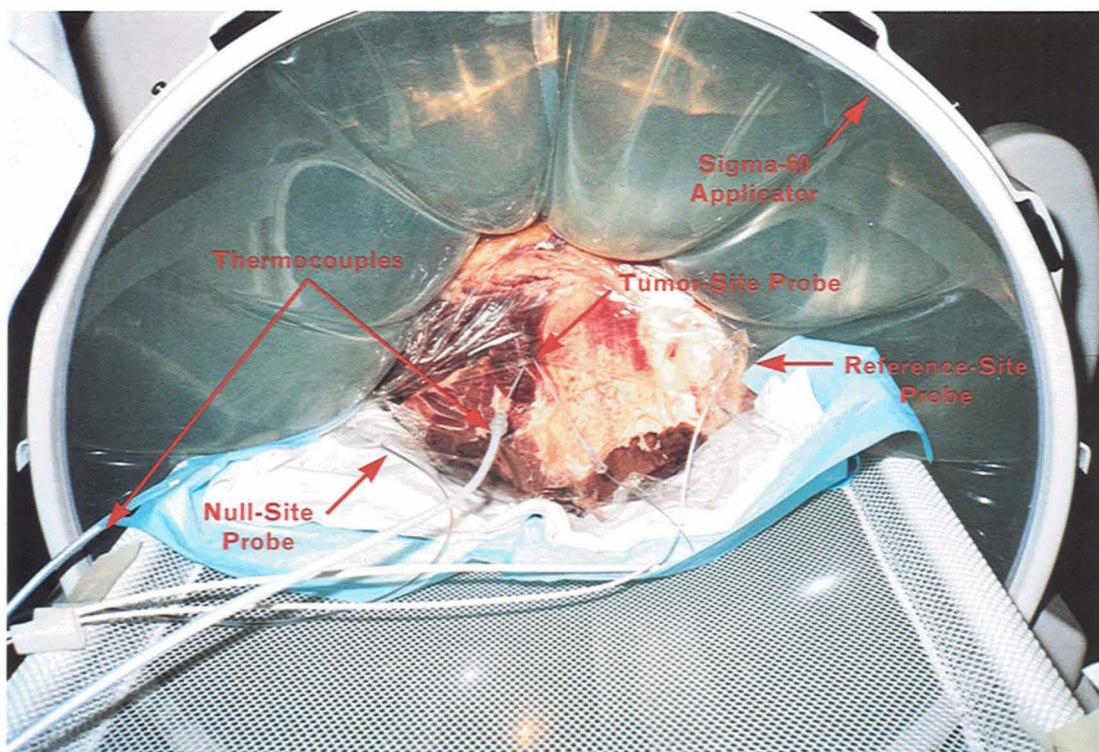


**FIGURE 7.** Beef-phantom target with electric-field probes and thermocouples.

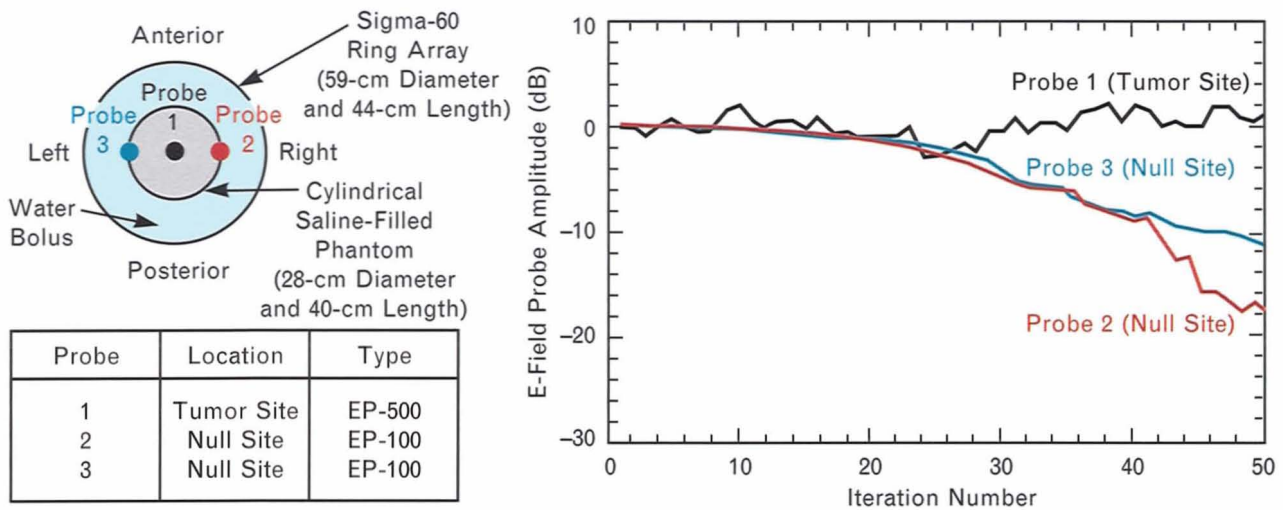


**FIGURE 8.** Experimental demonstration of adaptive nulling with the adaptive hyperthermia system at SUNY: (left) cross section of experimental configuration with saline-filled cylindrical phantom and (right) measured electric field as a function of adaptive-nulling gradient-search iteration number (frequency = 100 MHz). Note that two adaptive nulls were independently formed at the locations of probes 2 and 3 while the power at probe 1 was kept relatively constant.

mit forward powers for channels 1 through 4 were 163 W, 390 W, 170 W, and 112 W, respectively, and the corresponding phase shifts were 76°, 60°, 58°, and 131°, respectively. The measured electric field as a function of iteration number is displayed in Figure 11. Note that the null-site probe power decreases during the first 30 iterations, after which the average null-site amplitude (cancellation) is about

-20 dB. The tumor-site power drops by about 2 dB during the 50 iterations; the power reduction is attributed in part to a shift in the beam peak away from the focus. The power at the reference site increases by about 2 dB during the 50 iterations; the increase is consistent with the assumption that the beam peak shifts away from the focus.

To record calibrated thermocouple data, we

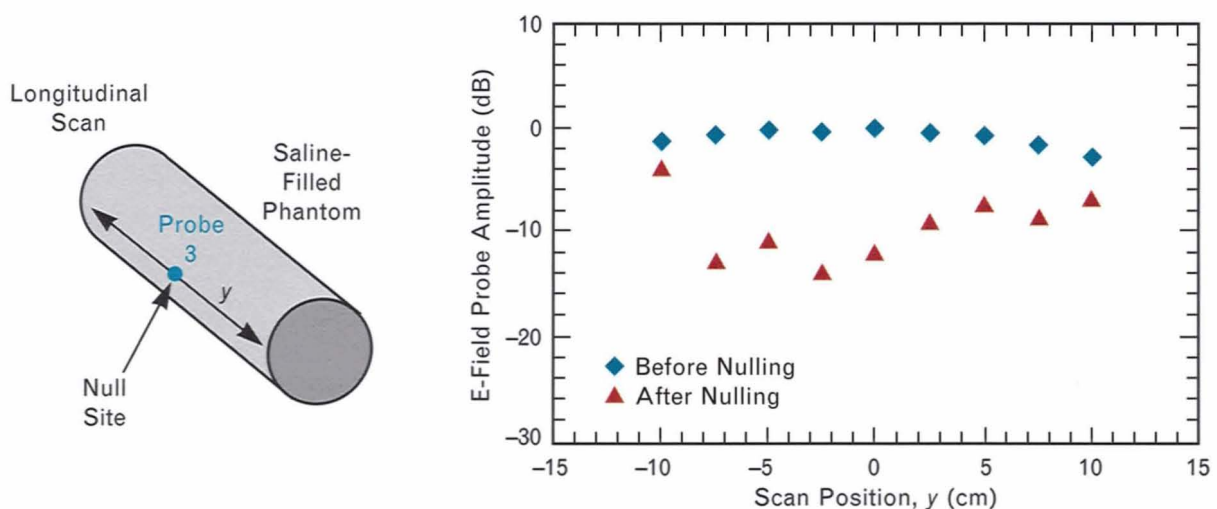


**FIGURE 9.** Experimental demonstration of adaptive nulling with the adaptive hyperthermia system at SUNY: (left) experimental configuration with saline-filled cylindrical phantom and (right) measured electric field on the surface of the cylindrical phantom before and after nulling (frequency = 100 MHz). The experiment uses the setup shown in Figure 8, except the position of probe 3 is moved longitudinally over a distance of 20 cm.

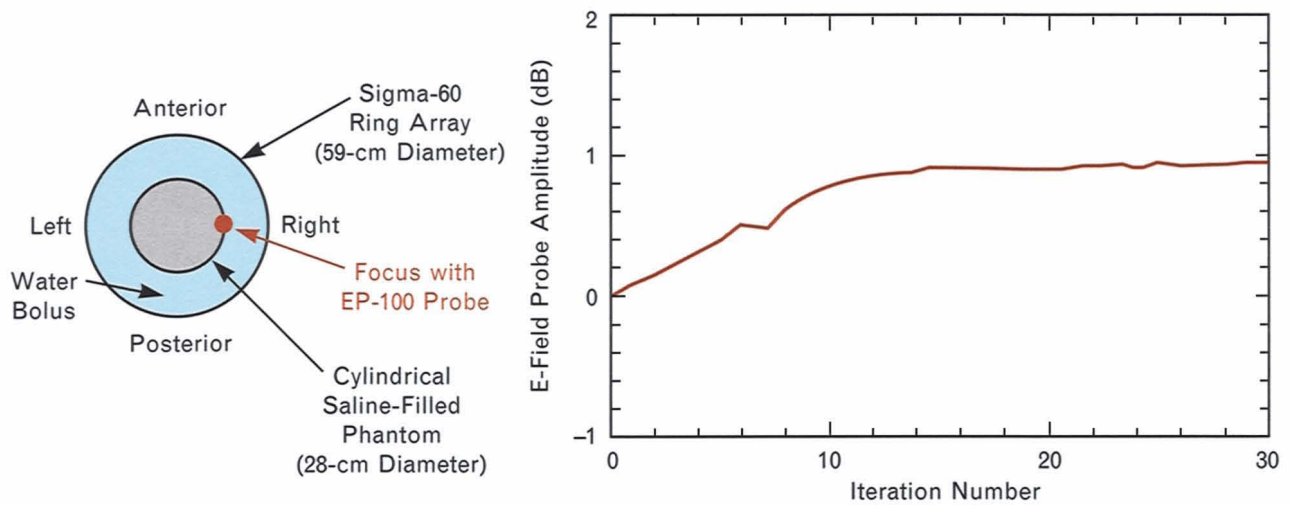


**FIGURE 10.** Experimental demonstration of adaptive focusing with the adaptive hyperthermia system at SUNY: (left) cross section of experimental configuration with saline-filled cylindrical phantom and (right) measured electric field as a function of adaptive-phase-focusing gradient-search iteration number (frequency = 100 MHz). The power level at the focus increases by 0.8 dB due to the adaptive gradient search.

turned the RF antenna off for about 5 min after every 10 iterations. (Note: The length of time for 10 iterations is approximately 12 min with the present software/hardware configuration. A faster iteration speed is required for the practical use of the gradient-search algorithm in patient therapy. Optimizing the software/hardware configuration for adaptive feedback operation should enable faster speeds.) During the

period when the RF antenna was off, the temperature-monitoring mode of the BSD-2000 system was accessed and the data recorded. The RF antenna was then turned back on with the transmit weights set to values of the previous iteration. Figure 12 shows the experimental configuration used and the measured temperatures at the tumor and null sites. The initial temperatures were approximately equal; after 80 min

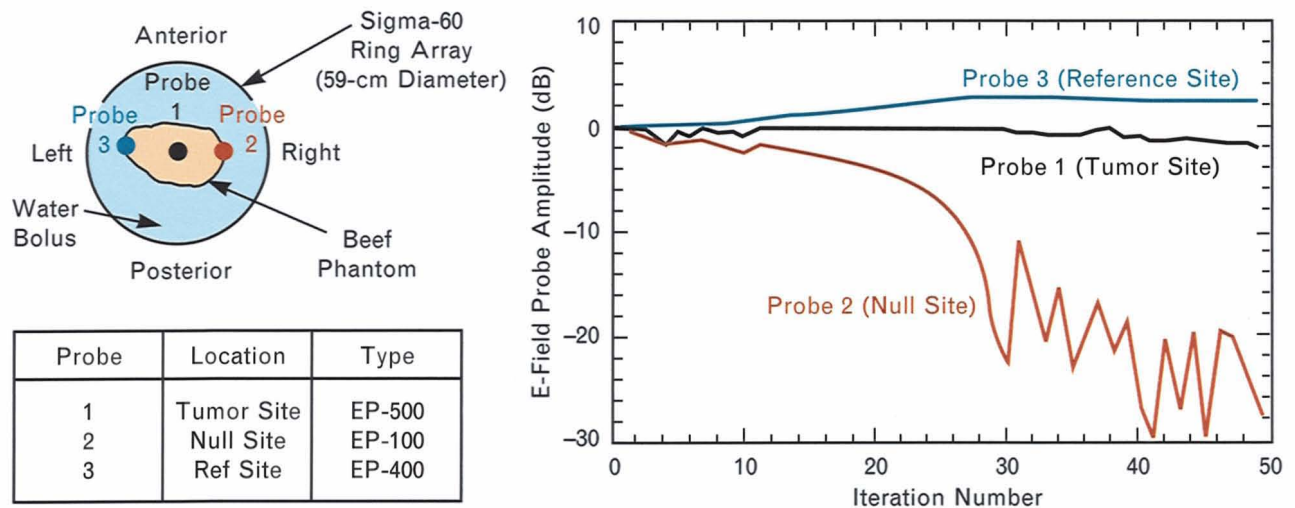


**FIGURE 11.** Experimental demonstration of adaptive nulling with the adaptive hyperthermia system at SUNY: (left) cross section of experimental configuration with beef phantom and (right) measured electric field as a function of adaptive-nulling gradient-search iteration number (frequency = 120 MHz). Note that one adaptive null is formed at the location of probe 2 while the power level at the location of probe 1 (the tumor site) is maintained within 2 dB.

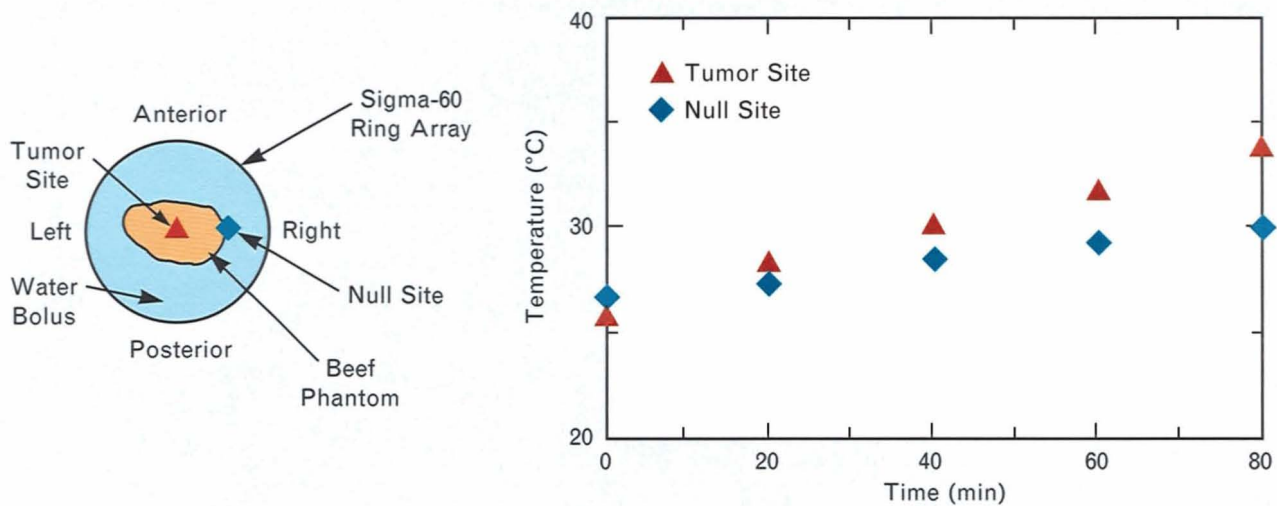


**FIGURE 12.** Experimental demonstration of the adaptive hyperthermia system at SUNY: (left) cross section of experimental configuration with beef phantom and (right) measured temperatures in the phantom (frequency = 120 MHz). After 80 min, the temperature at the tumor site is 4°C higher than that at the null site. (Note: The RF antenna was turned off for approximately 5-min intervals during the temperature measurements.)

the temperature at the tumor site was 4°C higher than that at the null site. Thus the data suggest that adaptive nulling can be effective in improving the thermal distribution in hyperthermia treatment. For the future, more detailed thermal measurements in three dimensions are planned.

### Conclusion

We have investigated the use of adaptive array antenna techniques in the hyperthermia treatment of cancer. Both computer simulations and experimental measurements have shown that adaptive nulling can be used to prevent undesired hot spots from occurring during the heating of a deep-seated tumor by a hyperthermia annular phased-array system.

For the experimental measurements, we used a BSD-2000 Sigma-60 hyperthermia system at the State University of New York (SUNY) Health Science Center in Syracuse, N.Y. The commercial phased-array system was modified to implement adaptive-nulling and adaptive-focusing algorithms. The experimental measurements reported in this article demonstrate that the electric-field radiation pattern of a hyperthermia phased array can be controlled by an adaptive algorithm. Both electric-field nulling (power minimization) and focusing (power maximization) at desired phantom target positions were experimentally

demonstrated. Although the emphasis of our experiments was on electric-field measurements, limited beef-phantom temperature data were also measured and reported.

The purpose of electric-field nulling is to reduce the occurrence of undesired hot spots inside or on the surface of a target body. In contrast, electric-field focusing is intended to maximize the RF power delivered to a tumor site. The data presented in this article suggest that both these goals can be achieved with an adaptive hyperthermia phased-array system. A potential clinical application of the adaptive phased-array system has been outlined.

In the experiments, the adaptive algorithm used was a gradient-search feedback technique (method of steepest descent/ascent). For RF nulling, the gradient search employed transmit-weight amplitude and phase dithering together with probe measurements of the electric-field power at the desired target positions to calculate the required gradient-search directions. For RF focusing, a phase-only transmit-weight dithering algorithm was used. Short-dipole electric-field sensors provided the feedback amplitude signals for the adaptive array. Two phantom targets were investigated in the experiments: a homogeneous saline-filled cylindrical target and a heterogeneous (tissue, bone, and fat) beef target. For the saline-filled phantom

target, two independent adaptive electric-field nulls were demonstrated at 100 MHz. In addition, the electric-field longitudinal surface distribution was measured before and after adaptive nulling. The longitudinal field-probe measurements indicated a finite-width null characteristic. The saline-filled phantom was also used to demonstrate adaptive focusing on the surface of the phantom. For the beef sample, one adaptive null was obtained at 120 MHz. During the adaptive-nulling beef-phantom testing, the measured thermocouple data indicated that the temperature at the tumor site was 4°C higher than the temperature at the target surface. The measured adaptive null strengths were on the order of -10 to -30 dB. For practical implementation of the adaptive-nulling algorithm, the required minimum null strength for local near-surface hot-spot reduction is assumed to be on the order of -3 to -6 dB, which we readily achieved.

The data from our experiments are encouraging.

The results indicate that adaptive-nulling and adaptive-focusing array control can potentially improve the hyperthermia treatment of cancer patients. Further experiments are planned.

### **Acknowledgments**

The support of the Lincoln Laboratory Advanced Concepts Committee is sincerely appreciated. Technical discussions with P.F. Turner and the software support of J. Robbins, both of BSD Medical Corp., have been very helpful in this study. The authors are also grateful to D.H. Temme and D.M. Nathanson of Lincoln Laboratory for technical discussions and to J.F. Fitzgerald and L.S. Dipalma for technical assistance.

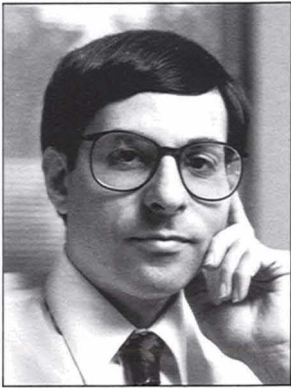
This work was sponsored by the Department of the Air Force.

*(Editor's note: A revised and abridged version of this article has been submitted to the International Journal of Hyperthermia.)*

## REFERENCES

1. C.A. Perez and L.W. Brady, *Principles and Practice of Radiation Oncology* (J.B. Lippincott, Philadelphia, 1987).
2. S.B. Field and J.W. Hand, *An Introduction to the Practical Aspects of Clinical Hyperthermia* (Taylor & Francis, New York, 1990).
3. A.W. Guy, "History of Biological Effects and Medical Applications of Microwave Energy," *IEEE Trans. Microwave Theory Tech.* **32**, 1182 (1984).
4. J. Overgaard, "Clinical Hyperthermia—An Update," *Radiation Research, Proc. 8th Int. Congress of Radiation Research 2, Jul. 1987*, eds. E.M. Fielden, J.F. Fowler, J.H. Hendry, and D. Scott, p. 942.
5. J. Overgaard, "The Effect of Local Hyperthermia Alone, and in Combination with Radiation on Solid Tumors," in *Cancer Therapy by Hyperthermia and Radiation, Proc. 2nd Int. Symp., 2-4 June 1977*, ed. C. Streffer (Urban & Schwarzenberg, Baltimore, 1978), p. 49.
6. A.R. von Hippel, A.H. Runck, and W.B. Westphal, "Dielectric Analysis of Biomaterials," *Technical Report 13*, MIT Laboratory for Insulation Research (Oct. 1973), pp. 16-19, DTIC #AD-769843.
7. J.C. Lin, ed., "Special Issue on Phased Arrays for Hyperthermia Treatment of Cancer," *IEEE Trans. Microwave Theory Tech.* **34**, 481 (1986).
8. J.W. Strohbehn, T.C. Cetas, and G.M. Hahn, eds., "Special Issue on Hyperthermia and Cancer Therapy," *IEEE Trans. Biomed. Eng.* **3**, 1 (1984).
9. P.F. Turner, T. Schaefermeyer, and T. Saxton, "Future Trends in Heating Technology of Deep-Seated Tumors," *Recent Results Cancer Res.* **107**, 249 (1988).
10. P.F. Turner, A. Tumeh, and T. Schaefermeyer, "BSD-2000 Approach for Deep Local and Regional Hyperthermia: Physics and Technology," *Strahlentherapie Onkologie* **165**, 738 (1989).
11. M.I. Skolnik, *Introduction to Radar Systems*, 2nd ed. (McGraw-Hill, New York, 1980).
12. R.T. Compton, Jr., *Adaptive Antennas: Concepts and Performance* (Prentice Hall, Englewood Cliffs, NJ, 1988).
13. V. Sathiaselan, M.F. Iskander, G.C.W. Howard, and N.M. Bleehen, "Theoretical Analysis and Clinical Demonstration of the Effect of Power Pattern Control Using the Annular Phased-Array Hyperthermia System," *IEEE Trans. Microwave Theory Tech.* **34**, 514 (1986).
14. V. Sathiaselan, "Potential for Patient-Specific Optimization of Deep Heating Patterns through Manipulation of Amplitude and Phase," *Strahlentherapie Onkologie* **165**, 743 (1989).
15. D. Sullivan, "Three-Dimensional Computer Simulation in Deep Regional Hyperthermia Using the Finite-Difference Time-Domain Method," *IEEE Trans. Microwave Theory Tech.* **38**, 204 (1990).
16. D. Sullivan, "Mathematical Methods for Treatment Planning in Deep Regional Hyperthermia," *IEEE Trans. Microwave Theory Tech.* **39**, 864 (1991).
17. B.S. Trembly, A.H. Wilson, M.J. Sullivan, A.D. Stein, T.Z. Wong, and J.W. Strohbehn, "Control of the SAR Pattern within an Interstitial Microwave Array through Variation of Antenna Driving Phase," *IEEE Trans. Microwave Theory Tech.* **34**, 568 (1986).
18. G. Sato, C. Shibata, S. Sekimukai, H. Wakabayashi, K. Mitsuoka, and K. Giga, "Phase-Controlled Circular Array Heating Equipment for Deep-Seated Tumors: Preliminary Experiments," *IEEE Trans. Microwave Theory Tech.* **34**, 520 (1986).
19. P.A. Cudd, A.P. Anderson, M.S. Hawley, and J. Conway, "Phased-Array Design Considerations for Deep Hyperthermia through Layered Tissue," *IEEE Trans. Microwave Theory Tech.* **34**, 526 (1986).
20. D.B. Nguyen and J.W. Strohbehn, "Optimal Positions, Orientations, Amplitudes and Phases of Movable Microwave Applicators in Hyperthermia Treatment," in *Hyperthermic Oncology 1988, Vol. 1*, eds. T. Sugahara and M. Saito (Taylor & Francis, London, 1989), pp. 738-739.
21. C. De Wagter, "Optimization of Simulated Two-Dimensional Temperature Distributions Induced by Multiple Electromagnetic Applicators," *IEEE Trans. Microwave Theory Tech.* **34**, 589 (1986).
22. M. Knudsen and U. Hartmann, "Optimal Temperature Control with Phased Array Hyperthermia System," *IEEE Trans. Microwave Theory Tech.* **34**, 597 (1986).
23. C.F. Babbs, V.A. Vaguine, and J.T. Jones, "A Predictive-Adaptive, Multipoint Feedback Controller for Local Heat Therapy of Solid Tumors," *IEEE Trans. Microwave Theory Tech.* **34**, 604 (1986).
24. R.B. Roemer, "Physical and Engineering Aspects of Hyperthermia," *Radiation Research, Proc. 8th Int. Congress of Radiation Res. 2, Jul. 1987*, eds. E.M. Fielden, J.F. Fowler, J.H. Hendry, and D. Scott, p. 948.
25. R.B. Roemer, J. Hynynen, C. Johnson, and R. Kress, "Feedback Control and Optimization of Hyperthermia Heating Patterns: Present Status and Future Needs," *IEEE 8th Ann. Conf. of Eng. in Medicine and Biology Soc., Fort Worth, TX, Nov. 1986*, p. 1496.
26. A. Boag and Y. Leviatan, "Optimal Excitation of Multiapplicator Systems for Deep Regional Hyperthermia," *IEEE Trans. Biomed. Eng.* **37**, 987 (1990).
27. J.T. Loane III and S.-W. Lee, "Gain Optimization of a Near-Field Focusing Array for Hyperthermia Applications," *IEEE Trans. Microwave Theory Tech.* **37**, 1629 (1989).
28. N. Morita, T. Hamasaki, and N. Kumagai, "An Optimal Excitation Method in Multiapplicator Systems for Forming a Hot Zone inside the Human Body," *IEEE Trans. Microwave Theory Tech.* **34**, 532 (1986).
29. P. Wust, J. Nadobny, R. Felix, P. Deuffhard, A. Louis, and W. John, "Strategies for Optimized Application of Annular-Phased-Array Systems in Clinical Hyperthermia," *Int. J. Hyperthermia* **7**, 157 (Jan.-Feb. 1991).
30. J.W. Strohbehn, E.H. Curtis, K.D. Paulsen, X. Yuan, and D.R. Lynch, "Optimization of the Absorbed Power Distribution for an Annular Phased Array Hyperthermia System," *Int. J. Radiation Oncology, Biology, Physics* **16**, 589 (1989).
31. A.J. Fenn, "Evaluation of Adaptive Phased-Array Antenna Far-Field Nulling Performance in the Near-Field Region," *IEEE Trans. Antennas Propag.* **38**, 173 (1990).
32. A.J. Fenn, "Near-Field Testing of Adaptive Radar Systems," *Proc. 12th Ann. Antenna Measurement Techniques Assoc. Mtg. and Symp., 8-11 Oct. 1990*, p. 13-9.
33. A.J. Fenn, "Theory and Analysis of Near Field Adaptive Nulling," *1986 IEEE Antennas Propag. Soc. Int. Symp. Dig. 2, Philadelphia, 9-13 June 1986*, p. 579.
34. A.J. Fenn, H.M. Aumann, F.G. Willwerth, and J.R. Johnson, "Focused Near-Field Adaptive Nulling: Experimental Investigation," *1990 IEEE Antennas Propag. Soc. Int. Symp. Dig. 1, Dallas, 7-11 May 1990*, p. 186.
35. A.J. Fenn, "Adaptive Hyperthermia for Improved Thermal Dose Distribution," in *Radiation Research: A Twentieth-Century*

- ry Perspective, Vol. 1: Congress Abstracts, eds. J.D. Chapman, W.C. Dewey, and G.F. Whitmore (Academic Press, San Diego, CA, 1991), p. 290.
36. A.J. Fenn, "Focused Near-Field Nulling for Adaptive Electromagnetic Hyperthermia Applications," *Proc. Progress in Electromagnetics Research Symp., Cambridge, MA, 1-5 Jul. 1991*, p. 393.
  37. A.J. Fenn, "Application of Adaptive Nulling to Electromagnetic Hyperthermia for Improved Thermal Dose Distribution in Cancer Therapy," *Technical Report 917*, Lincoln Laboratory (3 Jul. 1991), DTIC #AD-A241026.
  38. A.J. Fenn, "Non-Invasive Adaptive Nulling for Improved Hyperthermia Thermal Dose Distribution," *IEEE Eng. in Medicine and Biology Soc. Int. Conf. 13, Orlando, FL, 31 Oct.-3 Nov. 1991*, p. 976.
  39. A.J. Fenn, "Application of Adaptive Nulling for Improving the Thermal Distribution in Electromagnetic Hyperthermia," submitted to the *Applied Computational Electromagnetics Soc. Special Issue on Bioelectromagnetic Computations* (1992).
  40. G.A. King and A.J. Fenn, "Adaptive Nulling Measurements with the BSD Sigma-60 Applicator for Improved Hyperthermia Thermal Distribution," *Hyperthermic Oncology 1992, Vol. 1, Summary Papers, Proc. 6th Int. Congress on Hyperthermic Oncology, 27 Apr.-1 May 1992*, ed. E.W. Gerner, p. 246.
  41. A.J. Fenn and G.A. King, "An Adaptive Radio-Frequency Hyperthermia Phased-Array System for Improved Cancer Therapy: Phantom Target Measurements," *Project Report ACC-3*, Lincoln Laboratory (30 Apr. 1992).
  42. R.C. Johnson and J. Jasik, *Antenna Engineering Handbook*, 2nd ed. (McGraw-Hill, New York, 1984), chap. 22.
  43. J.R. Johnson, A.J. Fenn, H.M. Aumann, and F.G. Willwerth, "An Experimental Adaptive Nulling Receiver Utilizing the Sample Matrix Inversion Algorithm with Channel Equalization," *IEEE Trans. Microwave Theory Tech.* **39**, 798 (1991).
  44. R.L. Zahradnik, *Theory and Techniques of Optimization for Practicing Engineers* (Barnes and Noble, New York, 1971), pp. 118-124.
  45. V.W.S. Chan, "A Fast Algorithm for Spatial Interference Rejection," *Int. Conf. on Communications 1, Seattle, June 1980*, p. 59.4.1.
  46. A. Cantoni, "Application of Orthogonal Perturbation Sequences to Adaptive Beamforming," *IEEE Trans. Antennas Propag.* **28**, 191 (1980).
  47. D.C. Farden and R.M. Davis, "Orthogonal Weight Perturbation Algorithms in Partially Adaptive Arrays," *IEEE Trans. Antennas Propag.* **33**, 56 (1985).
  48. D.J. Farina and R.P. Flam, "A Self-Normalizing Gradient Search Adaptive Array Algorithm," *IEEE Trans. Aerosp. & Electron. Syst.* **27**, 901 (1991).
  49. A.J. Fenn, "Maximizing Jammer Effectiveness for Evaluating the Performance of Adaptive Nulling Array Antennas," *IEEE Trans. Antennas Propag.* **33**, 1131 (1985).
  50. L.C. Godara and A. Cantoni, "Analysis of the Performance of Adaptive Beam Forming Using Perturbation Sequences," *IEEE Trans. Antennas Propag.* **31**, 268 (1983).
  51. J.H. Richmond, "Radiation and Scattering by Thin-Wire Structures in a Homogeneous Conducting Medium (Computer Program Description)," *IEEE Trans. Antennas Propag.* **22**, 365 (1974).
  52. J.H. Richmond, "Radiation and Scattering by Thin-Wire Structures in the Complex Frequency Domain," *Technical Report 2902-10*, Ohio State University, ElectroScience Laboratory, NTIS N74-21856 (July 1973).
  53. J.H. Richmond, "Computer Program for Thin-Wire Structures in a Homogeneous Conducting Medium," *Technical Report 2902-12*, Ohio State University, ElectroScience Laboratory (Aug. 1973).
  54. J.T. Bartoszek, B. Huckins, and M. Coyle, "A Simplified Shuttle Payload Thermal Analyzer (SSPTA) Program," *ALAA 14th Thermophysics Conf., 4-6 June 1979*.
  55. Y. Zhang, W.T. Joines, and J.R. Oleson, "The Calculated and Measured Temperature Distribution of a Phased Interstitial Antenna Array," *IEEE Trans. Microwave Theory Tech.* **38**, 69 (1990).
  56. H.I. Bassen and G.S. Smith, "Electric Field Probes—A Review," *IEEE Trans. Antennas Propag.* **31**, 710 (1983).
  57. A. Uhler, "Characterization of Crystal Diodes for Low-Level Microwave Detection," *Microwave J.* **6**, 59 (Jul. 1963).
  58. M. Astrahan, K. Imanaka, G. Jozsef, F. Ameye, L. Baert, M.D. Sapozink, S. Boyd, and Z. Petrovich, "Heating Characteristics of a Helical Microwave Applicator for Transurethral Hyperthermia of Benign Prostatic Hyperplasia," *Int. J. Hyperthermia* **7**, 141 (Jan.-Feb. 1991).
  59. C.K. Chou, G.W. Chen, A.W. Guy, and K.H. Luk, "Formulas for Preparing Phantom Muscle Tissue at Various Radio Frequencies," *Bioelectromagnetics* **5**, 435 (1984).



**ALAN J. FENN**

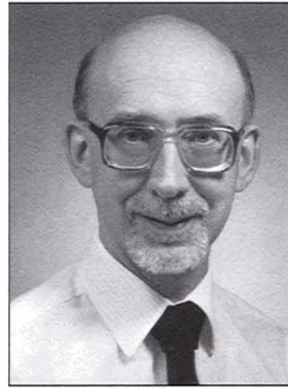
received the following degrees in electrical engineering: a B.S. in 1974 from the University of Illinois in Chicago and an M.S. and Ph.D. in 1976 and 1978, respectively, from Ohio State University in Columbus.

From 1974 to 1978 Alan was a graduate research associate at the Ohio State University ElectroScience Laboratory, where he did research in phased-array antenna analysis. He later became a senior engineer at Martin Marietta Aerospace in Denver, where he was involved in broadband antenna research and development from 1978 to 1981. He joined the staff of Lincoln Laboratory in 1981 and was a member of the Space Radar Technology Group from 1982 to 1991, where his research was in phased-array antenna design, adaptive-array near-field testing, and antenna and radar cross-section measurements. Since 1990 he has been conducting research in the application of adaptive-nulling techniques to RF hyperthermia

treatment. He is currently an assistant leader in the RF Technology Group, where he is investigating optoelectronic integrated-circuit phased-array antennas for mobile satellite communications applications.

In 1990 Alan was a co-recipient of the IEEE Antennas & Propagation Society's H.A. Wheeler Applications Prize Paper Award for "Phased Array Antenna Calibration and Pattern Prediction Using Mutual Coupling Measurements," a paper that he coauthored for the *IEEE Transactions on Antennas and Propagation*. He served as an associate editor in the area of adaptive arrays for the *IEEE Transactions on Antennas and Propagation* from 1989 to 1991. He is a senior member of the IEEE and has been appointed to a five-year term of membership in the Institute for Systems and Components of the Electromagnetics Academy.

He is the author or coauthor of more than 20 articles in his field and has presented more than 20 papers at national and international society meetings.



**GERALD A. KING**

studied electrical engineering and biology at the Rensselaer Polytechnic Institute in Troy, N.Y., and was a research fellow at the State University of New York (SUNY) Upstate Medical Center in Syracuse, N.Y., where he received an M.D. degree in 1965. He completed his internship at St. Joseph's Hospital in Syracuse and his residency at the Stanford University Medical Center in Palo Alto, Calif., and was certified in therapeutic radiology by the American Board of Radiology in 1970.

From 1969 to 1971, Jerry was the chief of radiation therapy service and director of residency training for radiation therapy at the Fitzsimmons General Hospital in Denver. In 1971, he returned to Syracuse, where he has been an attending radiation oncologist at the University Hospital, SUNY Health Science Center; the Veterans Administration Hospital; and the Crouse Irving Memorial Hospital. Since 1987 and 1988, respectively, he has

been the Associate Director of the Division of Radiation Oncology, University Hospital, SUNY Health Science Center in Syracuse, and the Director of the hospital's Hyperthermia Cancer Treatment and Research Center. Jerry has also been an assistant professor (1971–1976), associate professor (1976–1991), and professor (1991–present) of the SUNY Health Science Center's Department of Radiology, Radiation Oncology, College of Medicine.

He is a member of a number of professional societies, including the American Association for the Advancement of Science, the American Association of Physicists in Medicine, the New York Academy of Sciences, the American Society for Therapeutic Radiology & Oncology, the American Society of Clinical Oncology, the Radiation Research Society, and the North American Hyperthermia Society.

An associate editor of *Medical Physics*, he is the author or coauthor of more than 30 articles in his field and has presented nearly 50 papers at national and international society meetings.